Metabolism Clinical and Experimental 101 (2019) 153993

Contents lists available at ScienceDirect

Metabolism Clinical and Experimental

journal homepage: www.metabolismjournal.com

Active pyruvate dehydrogenase and impaired gluconeogenesis in orthotopic hepatomas of rats

Min Hee Lee [a], Ralph J. DeBerardinis [b], Xiaodong Wen [a], Ian R. Corbin [a], A. Dean Sherry [a,c,d], Craig R. Malloy [a,c,e,f], Eunsook S. Jin [a,e,*]

[a] Advanced Imaging Research Center, University of Texas Southwestern Medical Center, Dallas, TX 75390, USA
[b] Children's Medical Center Research Institute, University of Texas Southwestern Medical Center, USA
[c] Department of Radiology, University of Texas Southwestern Medical Center, USA
[d] Department of Chemistry, University of Texas at Dallas, Richardson, TX 75080, USA
[e] Department of Internal Medicine, University of Texas Southwestern Medical Center, USA
[f] VA North Texas Health Care System, Dallas, TX 75216, USA

ARTICLE INFO

Article history:
Received 14 August 2019
Accepted 7 October 2019

Keywords:
Hepatocellular carcinoma
Cancer metabolism
Pyruvate dehydrogenase
Pyruvate carboxylase
Tricarboxylic acid cycle
Glycerol

ABSTRACT

Background: Therapies targeting altered activity of pyruvate dehydrogenase (PDH) and pyruvate carboxylase (PC) have been proposed for hepatomas. However, the activities of these pathways in hepatomas in vivo have not been distinguished. Here we examined pyruvate entry into the tricarboxylic acid (TCA) cycle through PDH versus PC in vivo using hepatoma-bearing rats.

Methods: Hepatoma-bearing rats were generated by intrahepatic injection of H4IIE cells. Metabolism of ^{13}C-labeled glycerol, a physiological substrate for both gluconeogenesis and energy production, was measured with ^{13}C NMR analysis. The concentration of key metabolites and the expression of relevant enzymes were measured in hepatoma, surrounding liver, and normal liver.

Results: In orthotopic hepatomas, pyruvate entry into the TCA cycle occurred exclusively through PDH and the excess PDH activity compared to normal liver was attributed to downregulated pyruvate dehydrogenase kinase (PDK) 2/4. However, pyruvate carboxylation via PC and gluconeogenesis were minimal, which was linked to downregulated forkhead box O1 (FoxO1) by Akt activity. In contrast to many studies of cancer metabolism, lactate production in hepatomas was not increased which corresponded to reduced expression of lactate dehydrogenase. The production of serine and glycine in hepatomas was enhanced, but glycine decarboxylase was downregulated.

Conclusions: The combination of [U-$^{13}C_3$]glycerol and NMR analysis enabled investigation of multiple biochemical processes in hepatomas and surrounding liver. We demonstrated active PDH and other related metabolic alterations in orthotopic hepatomas that differed substantially not only from the host organ but also from many earlier studies with cancer cells.

Abbreviations: ACI, AxC-Irish; Ala, alanine; C/EBPα, CCAAT/enhancer-binding protein alpha; cDNA, complementary DNA; DHAP, dihydroxyacetone phosphate; DSS, 4,4-dimethyl-4-silapentane-1-sulfonic acid; FoxO1, forkhead box O1; GA3P, glyceraldehyde 3-phosphate; GAPDH, glyceraldehyde 3-phosphate dehydrogenase; G6Pase, glucose 6-phosphatase; GK, glycerol kinase; GLDC, glycine decarboxylase; Glu, glutamate; Gly, glycine; HIF-1α, hypoxia-inducible factor-1alpha; HRP, horseradish peroxidase; IGF, insulin-like growth factor; IR, insulin receptor; IRS, insulin receptor substrate; α-kG, alpha ketoglutarate; LDH, lactate dehydrogenase; MRI, magnetic resonance imaging; OAA, oxaloacetate; PC, pyruvate carboxylase; PDH, pyruvate dehydrogenase; PDK, pyruvate dehydrogenase kinase; PDP, pyruvate dehydrogenase phosphatase; PEP, phosphoenolpyruvate; PEPCK, phosphoenolpyruvate carboxykinase; PHGDH, 3-phosphoglycerate dehydrogenase; 3PG, 3-phosphoglycerate; RT–qPCR, real-time quantitative PCR; SHMT, serine hydroxymethyltransferase; PK, pyruvate kinase; PKM2, pyruvate kinase subtype M2; PSAT, phosphoserine aminotransferase; Ser, serine; Suc, succinate; TBS/T, tris-buffered saline with 0.1% Tween 20; TCA, tricarboxylic acid; THF, Tetrahydrofolate.

* Corresponding author at: Advanced Imaging Research Center, 5323 Harry Hines Blvd., Dallas, TX 75390-8568, USA.
E-mail address: Eunsook.Jin@utsouthwestern.edu (E.S. Jin).

https://doi.org/10.1016/j.metabol.2019.153993
0026-0495/

1. Introduction

Recent discoveries – oncometabolites, the role of mitochondria in cancer, metabolic heterogeneity in some tumors – have led to a resurgence of interest in cancer metabolism [1–3]. Analysis of metabolic pathways in hepatocellular carcinoma, one of the most common malignancies worldwide [4], is particularly challenging because of the metabolic flexibility of the host organ. Healthy liver uses simple molecules such as glycerol, alanine and lactate for energy production by metabolism to pyruvate, decarboxylation by pyruvate dehydrogenase (PDH) to acetyl-CoA, and subsequent oxidation in the tricarboxylic acid (TCA) cycle in mitochondria [5–7]. The liver also converts pyruvate to oxaloacetate, an intermediate of the TCA cycle, via pyruvate carboxylase (PC) to support biosynthetic processes including gluconeogenesis [6–8].

These alternate pathways for entry of pyruvate into the TCA cycle are the targets of recent strategies for hepatoma therapy [9–11]. Tumor growth rate and invasion are linked to excess lactate derived from pyruvate production through aerobic glycolysis, and directing pyruvate into the TCA cycle via PDH is a strategy in cancer treatment [11,12]. Stimulating PDH had the effect of inhibiting hepatoma cell growth and sensitizing cells to chemotherapy [9,10]. Pyruvate carboxylation in the liver also directs pyruvate into the TCA cycle where it serves an essential role in gluconeogenesis [11,13]. Restoring gluconeogenesis is another therapeutic strategy specifically for hepatomas [11] and an inverse relation between gluconeogenic enzyme activities and hepatoma growth rate has been reported [14]. Nonetheless, the relative importance of PC versus PDH for entry of pyruvate into the TCA cycle has not been evaluated in hepatomas, and it is unclear how these alternate entries of pyruvate are regulated in hepatomas in situ. In earlier studies, glycolysis in hepatoma cells was not different from most cancer cells and was associated with overwhelming lactate production [9,15,16]. In contrast, gluconeogenic enzymes in hepatoma cells were mostly downregulated [14,17]. However, a study using isolated, tumor-bearing livers found that gluconeogenesis from pyruvate and alanine via the TCA cycle was inhibited, but gluconeogenesis from glycerol was not altered [18]. This study, however, did not distinguish metabolism of the cancer from the non-malignant surrounding liver tissue. A significant challenge, in addition to distinguishing flux through PDH from PC in vivo, is evaluating these reactions in hepatomas versus nontumor-bearing liver in an in vivo exam.

Considering both carboxylation and decarboxylation of pyruvate is required for understanding metabolic reprogramming in hepatomas. The use of a ^{13}C stable isotope tracer and ^{13}C detection of metabolic products could be ideally suited for distinguishing PC activity from PDH. ^{13}C-labeled glucose has been widely used for metabolic studies in cancer or liver. Glucose tracers have the advantage of assessing glycolysis, but they do not allow examination of gluconeogenesis, a key hepatic function. In this study, ^{13}C-labeled glycerol was used to distinguish PDH activity from PC and to examine gluconeogenesis in orthotopic hepatomas produced by the intrahepatic inoculation of H4IIE cells in rats. The use of [U-$^{13}C_3$]glycerol is attractive because (i) glycerol is a physiological substrate and it is utilized predominantly by liver [19], (ii) gluconeogenesis from glycerol does not require metabolism in mitochondria and bypasses the requirement for the intact TCA cycle activity, and (iii) flux of glycerol carbons through the "lower" pathways of glycolysis leads to pyruvate, enabling detection of pyruvate alternate entries into the TCA cycle. We found that orthotopic hepatomas had markedly reprogrammed carbohydrate metabolism including pyruvate decarboxylation followed by oxidative phosphorylation, but minimal pyruvate carboxylation and gluconeogenesis. ^{13}C NMR analysis generally confirmed predictions based on measures of gene expressions and phosphorylation state of enzymes.

2. Material and methods

2.1. Animal studies

The study was approved by the Institutional Animal Care and Use Committee at the University of Texas Southwestern Medical Center. Male AxC-Irish (ACI) rats had free access to ad libitum feed and water, and were placed on a 12:12-hour day-night cycle. Rats (n = 10) received intrahepatic injections of rat hepatoma cells (H4IIE; 2×10^6 cells/10 μL) to establish orthotopic liver tumors. The progress of tumor growth was monitored by proton magnetic resonance imaging (^1H MRI), and tumors grew to ~10 mm-diameter at three weeks of intrahepatic inoculation of the cells (Fig. S1). These tumor-bearing ACI rats (n = 10) and healthy ACI rats (n = 6) were fasted beginning 10:00 AM for a 24-hour fast with free access to water. On the next day, all rats received [U-$^{13}C_3$]glycerol (50%; 100 mg/kg) intraperitoneally under isoflurane anesthesia. Rats quickly awakened and were active for 60 min before sacrifice under anesthesia. Blood was collected from the inferior vena cava. Tumors and liver tissues were dissected, freeze-clamped using liquid nitrogen, and kept at −80 °C until further processing.

2.2. Sample processing for NMR analysis

Ground liver tissue or tumors (3 g) were treated with perchloric acid (10%) to extract water soluble metabolites. If tumors were small (<2 g), tumors from two rats were combined. The acid mixtures were vortexed for 1 min, centrifuged, and supernatants were transferred to new tubes. The extraction was repeated after adding DI water to the precipitate. The extracts were neutralized with KOH, centrifuged, and supernatants were lyophilized prior to NMR acquisition.

2.3. Hepatoma cells treated with ^{13}C-labeled gluconeogenic substrates

H4IIE cells were incubated in DMEM supplemented with 5.5 mM glucose, 10% fetal bovine serum and penicillin/streptomycin at 37 °C and 5% CO_2 for 3 days. The cells were treated with [U-$^{13}C_3$]glycerol (2 mM) or [U-$^{13}C_3$]propionate (2 mM, 10 mM) for 8 h. Cells and media from two dishes (150 × 25 mm; n = 6 dishes for each tracer) were combined and metabolites were extracted using perchloric acid for NMR acquisition.

2.4. NMR spectroscopy

All NMR spectra were collected using a Varian INOVA 14.1 T spectrometer (Agilent, Santa Clara, CA) equipped with a 3-mm broadband probe with the observe coil tuned to ^{13}C (150 MHz). Dried extracts were dissolved in ^2H_2O (300 μL) containing 4,4-dimethyl-4-silapentane-1-sulfonic acid (DSS; 5 mM; NMR reference), centrifuged and supernatant was transferred to a 3-mm tube for NMR acquisition. ^{13}C NMR spectra were collected using a 45° pulse (5.0 μs), 34,965 Hz sweep width, 104,986 data points, and a 1.5-s interpulse delay at 25 °C. Proton decoupling was performed using a standard WALTZ-16 pulse sequence. Spectra were averaged ~23,000 scans requiring 20 h. All NMR spectra were analyzed using ACD/Labs NMR spectral analysis program (Advanced Chemistry Development, Inc., Toronto, Canada).

2.5. NMR assessment of metabolite concentration and ^{13}C enrichment

In ^{13}C NMR analysis of tissue extracts, the relative concentration of each metabolite was measured using natural abundant ^{13}C signal (singlet, S) normalized by a NMR reference (DSS). Multiplet (such as doublet) signals in spectra reflect excess ^{13}C enrichments in metabolites indicating ^{13}C transfers from [U-$^{13}C_3$]glycerol in this study. The ^{13}C enrichment in each metabolite was estimated by assuming a singlet as

natural abundance based on the low probability of forming single-labeled metabolite from exogenous [U-$^{13}C_3$]glycerol.

2.6. RNA extraction and real-time quantitative PCR (RT–qPCR) analysis

Total RNA was isolated from liver tissue or hepatomas using TRIzol (Ambion, Carlsbad, CA). Complementary DNA (cDNA) was synthesized from 1 μg total RNA with oligo-dT primers using high capacity cDNA reverse transcription kit according to the manufacturer's protocol (Applied Biosystems, Grand Island, NY) on the S1000™ Thermal cycler (Bio rad laboratories, Hercules, CA). RT–qPCR was performed with the iTaq™ Universal SYBR® Green Supermix (Bio rad laboratories, Hercules, CA) on the CFX384™ real time system (Bio rad laboratories). The PCR primers are shown in Supplemental Table 1. The results were normalized by housekeeping genes such as glyceraldehyde 3-phosphate dehydrogenase (GAPDH) and β-actin.

2.7. Immunoblot analysis

Tissue and whole cell lysates were prepared by RIPA buffer supplemented with a protease inhibitor cocktail and phosphatase inhibitor cocktail (Roche Diagnostics, Indianapolis, IN). Proteins were mixed with sodium dodecyl sulfate sample buffer and denatured by boiling for 5 min. Samples were separated by 8–15% SDS-PAGE gels and transferred onto a nitrocellulose membrane (Millipore, Billerica, MA). Membranes were blocked in 5% non-fat milk in tris-buffered saline with 0.1% Tween 20 (TBS/T) for 1 h. After blocking, the blots were incubated with primary antibody in diluted blocking buffer overnight at 4 °C and washed in TBS/T, and incubated with secondary antibodies conjugated with horseradish peroxidase (HRP) for 1 h at room temperature. Blots were developed using an immobilon western chemiluminescent HRP substrate (Millipore). Relative densities of bands were quantified with UN-SCAN-IT gel 6.1 software. The results were normalized to the α-tubulin intensity of the same sample.

2.8. Plasma glucose and insulin assay

Plasma glucose was estimated using glucose oxidase (YSI 2300 Glucose Analyzer; GMI, Inc). Insulin was measured using a rodent insulin ELISA kit (ALPCO).

2.9. Materials

[U-$^{13}C_3$]glycerol (99%) was obtained from Cambridge Isotopes (Andover, MA) and other common chemicals were purchased from Sigma-Aldrich. The following antibodies were used: PDH, pyruvate dehydrogenase kinase (PDK) 2/3/4, PC, Myc, and anti-goat IgG-HRP from Santa Cruz Biotechnology (Dallas, TX); p-PDH (Ser293) from Millipore (Billerica, MA); PDK1 from Enzo Life Sciences (Farmingdale, NY); pyruvate kinase subtype M2 (PKM2), p-PKM2 (Tyr105), lactate dehydrogenase A (LDHA), Akt, p-Akt (Thr308), p-Akt (Ser473), forkhead box O1 (FoxO1), and p-FoxO1 (Ser256) from Cell signaling (Beverly, MA); α-tubulin, pyruvate dehydrogenase phosphatase (PDP) 2, rabbit IgG HRP linked whole Ab, and mouse IgG HRP linked whole Ab from Sigma (St. Louis, MO).

2.10. Statistical analysis

Values are presented as mean ± standard deviation (SD). Comparisons between groups were performed using two-tailed Student's *t*-test, where $p < 0.05$ was considered significant.

3. Results

3.1. Hepatoma-bearing rats are produced using H4IIE cell inoculation

Tumors grew to ~10 mm-diameter at three weeks after intrahepatic inoculation of H4IIE cells (Fig. S1). These hepatoma-bearing rats and healthy rats as controls had similar body weight, liver weight, plasma glucose and insulin concentrations after a fast (Table S2). All animals

Table 1
Relative concentrations and ^{13}C enrichments of metabolites. ^{13}C NMR analysis was performed with tissue extracts from the liver of healthy rats (**L**), non-malignant surrounding liver tissue (**ST**) and hepatomas (**H**) of tumor-bearing rats. The relative concentration of a metabolite was measured using a signal from natural ^{13}C abundance normalized by a NMR reference. Excess ^{13}C enrichment in each metabolite was calculated by assuming a singlet as natural abundance (1.1%).

Metabolite	Chemical shift	Control (n = 6)	Tumor-bearing rat (n = 10)		p value		
		Liver (n = 6)	**S**urrounding **T**issue (n = 10)	**H**epatoma (n = 7)[a]	**L** vs. **ST**	**L** vs. **H**	**ST** vs. **H**
Glucose (α & β; C1)	92.9 & 97.0 ppm	1.00 ± 0.14	0.97 ± 0.27	0.27 ± 0.08	0.806	<0.001	<0.001
Glucose enrichment (%)		6.91 ± 0.98	6.03 ± 0.69	4.53 ± 0.32	0.052	<0.001	<0.001
Glycerol (C1 & C3)	63.5 ppm	1.00 ± 0.26	0.54 ± 0.32	3.14 ± 0.88	0.014	<0.001	<0.001
[U-$^{13}C_3$]glycerol		1.00 ± 0.56	0.34 ± 0.15	1.45 ± 1.44	0.003	0.487	0.027
Glycerol enrichment (%)		17.4 ± 5.7	14.6 ± 9.5	8.0 ± 5.6	0.555	0.016	0.130
Glycerol 3-phosphate (C1)	63.3 ppm	1.00 ± 0.12	1.04 ± 0.24	0.32 ± 0.08	0.742	<0.001	<0.001
[U-$^{13}C_3$]G3P		1.00 ± 0.19	0.85 ± 0.28	0.18 ± 0.05	0.269	<0.001	<0.001
G3P enrichment (%)		2.77 ± 0.51	2.31 ± 0.24	1.69 ± 0.53	0.035	0.004	0.005
Serine (C2)	57.4 ppm	1.00 ± 0.38	1.49 ± 0.70	6.64 ± 2.33	0.138	<0.001	<0.001
Serine enrichment (%)		ND	ND	0.49 ± 0.13			
Taurine (C1)	48.6 ppm	1.00 ± 0.13	1.15 ± 0.66	1.25 ± 0.13	0.479	0.004	0.690
Glutathione (glycine unit C2)	44.4 ppm	1.00 ± 0.17	0.95 ± 0.09	0.71 ± 0.10	0.450	0.003	<0.001
Glycine (C2)	42.6 ppm	1.00 ± 0.08	1.08 ± 0.22	2.17 ± 0.45	0.395	<0.001	<0.001
Glycine enrichment (%)		0.14 ± 0.05	0.19 ± 0.08	0.74 ± 0.07	0.131	<0.001	<0.001
Phosphoethanolamine (N)	41.8 ppm	1.00 ± 0.23	1.20 ± 0.21	9.63 ± 1.52	0.104	<0.001	<0.001
Succinate (C2 & C3)	35.0 ppm	1.00 ± 0.23	1.22 ± 0.19	0.35 ± 0.05	0.051	<0.001	<0.001
Succinate enrichment by [$^{13}C_3$] (%)		0.34 ± 0.08	0.35 ± 0.09	ND	0.882		
Succinate enrichment by [$^{13}C_2$] (%)		0.15 ± 0.05	0.15 ± 0.04	0.26 ± 0.07	0.919	0.009	0.002
Glutamate (C4)	34.0 ppm	1.00 ± 0.08	0.93 ± 0.12	1.26 ± 0.12	0.230	<0.001	<0.001
Glutamate enrichment (%)		ND	ND	0.43 ± 0.08			
Glutamine (C4)		1.00 ± 0.09	0.88 ± 0.19	0.61 ± 0.10	0.159	<0.001	0.004
Glutamine enrichment (%)		ND	ND	0.05 ± 0.05			
β-Hydroxybutyrate (C4)	22.7 ppm	1.00 ± 0.14	0.84 ± 0.15	0.63 ± 0.08	0.052	<0.001	0.005
Lactate (C3)	21.0 ppm	1.00 ± 0.26	1.34 ± 0.21	1.51 ± 0.24	0.012	0.004	0.140
Lactate enrichment (%)		3.43 ± 0.52	3.05 ± 0.35	2.37 ± 0.07	0.097	<0.001	<0.001
Alanine C3	17.3 ppm	1.00 ± 0.22	1.23 ± 0.16	0.83 ± 0.08	0.031	0.081	<0.001
Alanine enrichment (%)		3.41 ± 0.46	2.94 ± 0.37	2.17 ± 0.10	0.041	<0.001	<0.001

[a] Total seven hepatoma samples were prepared from ten tumor-bearing rats by combining small tumors for NMR analysis; ND, not detected; data are represented as mean ± SD.

received [U-$^{13}C_3$]glycerol and data were collected on tissue extracts derived from three sources: 1) liver of healthy rats, 2) non-malignant surrounding liver tissue from hepatoma-bearing rats, and 3) hepatomas. Together 1) and 2) are referred as 'the liver' in this study since the results from both sources were similar in most assays. Overall [U-$^{13}C_3$] glycerol utilization in these sources can be estimated using the data in Table 1 showing the concentrations of metabolites of interest and their enrichments by ^{13}C-labeled ones.

3.2. Pyruvate enters the TCA cycle preferentially through PDH in hepatomas

[U-$^{13}C_3$]pyruvate derived from [U-$^{13}C_3$]glycerol has several fates through PDH, PC, lactate dehydrogenase (LDH) and alanine transaminase. The entry of [U-$^{13}C_3$]pyruvate to the TCA cycle through PC produces [1,2,3-$^{13}C_3$]oxaloacetate that undergoes rapid exchange with succinate (a symmetric molecule) producing equal amounts of [1,2,3-$^{13}C_3$] and [2,3,4-$^{13}C_3$]succinate (Fig. 1A). These triple-labeled molecules were detected in the liver by ^{13}C NMR [20], but not in hepatomas. The concentration of succinate was also substantially decreased in hepatomas (Fig. 1B). In contrast, the entry of [U-$^{13}C_3$]pyruvate through PDH produces [1,2-$^{13}C_2$]acetyl-CoA, and subsequent condensation with oxaloacetate produces [4,5-$^{13}C_2$]citrate and [4,5-$^{13}C_2$]α-ketoglutarate in the TCA cycle. Since α-ketoglutarate is in exchange with glutamate, the presence of [4,5-$^{13}C_2$]glutamate reflects PDH activity (Fig. 1A). [4,5-$^{13}C_2$]glutamate was detected in hepatomas only, and the concentration of glutamate was higher in hepatomas than the liver (Fig. 1C).

Consistent with NMR data, protein and mRNA expression of PC were lower in hepatomas compared to the liver (Fig. 2A). The activity of PDH is regulated through phosphorylation and dephosphorylation of its subunits by PDK and PDP, respectively [21–23]. In immunoblot analysis,

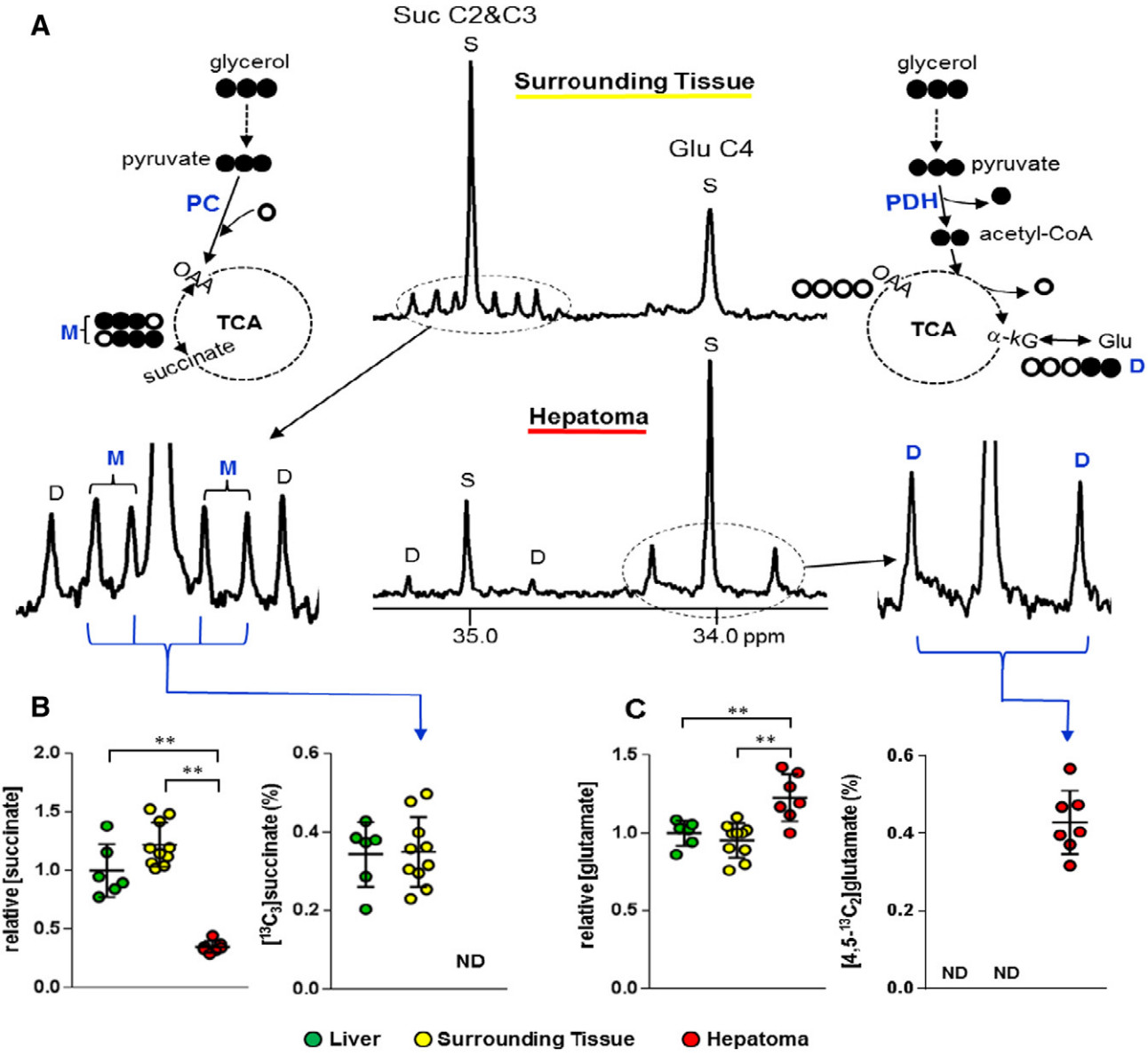

Fig. 1. Pyruvate decarboxylation in hepatomas versus pyruvate carboxylation in the liver. (A) [U-$^{13}C_3$]glycerol is directed to glycolysis becoming [U-$^{13}C_3$]pyruvate. The entry of [U-$^{13}C_3$] pyruvate to the TCA cycle through PC (carboxylation) produces triple-labeled ([1,2,3-$^{13}C_3$] or [2,3,4-$^{13}C_3$]) four-carbon units including oxaloacetate and succinate while the entry through PDH (decarboxylation) leads to double-labeled ([4,5-$^{13}C_2$]) α-ketoglutarate that is in exchange with glutamate. In ^{13}C NMR, triple-labeled succinate is detected in the liver only while double-labeled glutamate detected in hepatomas only. A singlet (S) is signal from natural ^{13}C abundance reflecting a pool size while a multiplet (D or M) is evidence of ^{13}C transfer from [U-$^{13}C_3$]glycerol. (B) The concentration of succinate is lower in hepatomas than the liver, and triple-labeled succinate is detected in the liver only. (C) The concentration of glutamate is higher in hepatomas than the liver, and double-labeled glutamate is detected in hepatomas only. Abbreviations: D, doublet from coupling of ^{13}C with adjacent ^{13}C; M, multiplet signal from [1,2,3-$^{13}C_3$] or [2,3,4-$^{13}C_3$]succinate; ND, not detected; S, singlet; open circle = ^{12}C; black circle = ^{13}C; **, $p < 0.001$; data are represented as mean ± SD.

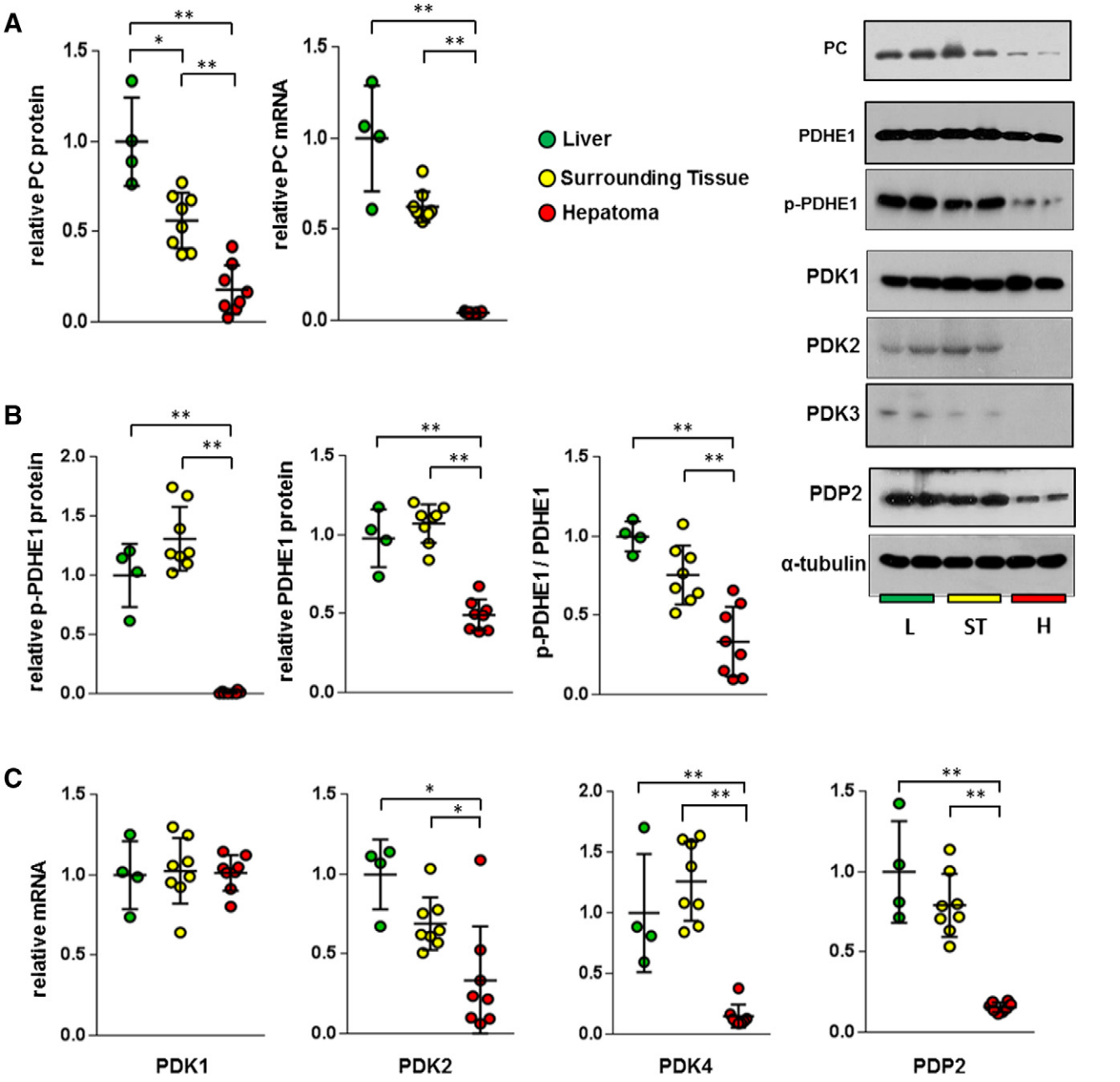

Fig. 2. Active PDH and downregulated PDK2/4 in hepatomas. (A) Protein and mRNA expression of PC are lower in hepatomas than the liver. (B) Proteins of PDHE1 and p-PDHE1, and the ratio of p-PDHE1/PDHE1 all are lower in hepatomas compared to the liver. (C) Protein and mRNA expression of PDK1 remain unchanged, but those of PDK2/4 are reduced in hepatomas. Gene expression of PDP2 is also reduced in hepatomas. Abbreviations: p-PDH, phosphorylated PDH; *, $p < 0.05$; **, $p < 0.001$; data are represented as mean ± SD.

phosphorylated PDHE1α (p-PDHE1) on serine 293 was dramatically lower and the ratio of p-PDHE1/PDHE1 was also lower in hepatomas compared to the liver (Fig. 2B). Protein and/or mRNA expressions of PDK2/4 were lower in hepatomas compared to the liver, but PDK1 remained unchanged (Fig. 2C). The expressions of PDK3 were trivial in all tissues, so they were not considered further in analysis. Gene expression of PDP2 was also decreased in hepatomas (Fig. 2C). Downregulated PDK2/4 was consistent with low p-PDHE1 and pyruvate decarboxylation proven by NMR, but downregulated PDP2 was contrary to the observations.

3.3. Gluconeogenesis is minimal in hepatomas

Glycerol after phosphorylation can be converted to dihydroxyacetone phosphate (DHAP) or glyceraldehyde 3-phosphate (GA3P). Condensation of DHAP and GA3P leads to glucose production, and triple-labeled ([1,2,3-$^{13}C_3$] or [4,5,6-$^{13}C_3$]) glucose in this study is evidence of gluconeogenesis from [U-$^{13}C_3$]glycerol (Fig. 3A). Both glucose concentration and its ^{13}C-enrichment were lower in hepatomas compared to the liver, demonstrating minimal gluconeogenesis from glycerol (Fig. 3B). Also mRNA expressions of glucose 6-phosphatase (G6Pase), phosphoenolpyruvate carboxykinase (PEPCK) and CCAAT/enhancer-binding protein alpha (C/EBPα) were decreased in hepatomas (Fig. 3C). C/EBPα is known to regulate gluconeogenic enzymes [24].

In addition to rat models, H4IIE cells were treated with ^{13}C-labeled gluconeogenic substrates (i.e., [U-$^{13}C_3$]glycerol or [U-$^{13}C_3$]propionate). [U-$^{13}C_3$]glycerol incorporated into glycine in these cells, but not into glucose (Fig. 4D). [U-$^{13}C_3$]propionate enters the TCA cycle through propionyl-CoA carboxylase and ultimately succinyl-CoA, labeling the cycle intermediates and exchanging pools. Thus the detection of ^{13}C-labeled

glucose after the administration of [U-$^{13}C_3$]propionate is evidence of gluconeogenesis from the TCA cycle. The entry of [U-$^{13}C_3$]propionate into the TCA cycle was evidenced by excess ^{13}C enrichment in glutamate that is in exchange with α-ketoglutarate, but again excess ^{13}C was not detected in glucose (data not shown). Together, these results indicate that gluconeogenesis from either glycerol or the TCA cycle was minimal in hepatomas with downregulated gluconeogenic enzymes.

3.4. FoxO1 is downregulated by Akt in hepatomas

Insulin signaling pathways were investigated if they are linked to metabolic alterations in liver tumors. Hepatomas had 4-fold higher mRNA expression of insulin receptor substrate 2 (IRS2) while they had lower expressions of insulin-like growth factor 1 (IGF1), IGF2, insulin receptor (IR), IGF1R and IRS1 compared to the liver (Fig. 4A). The protein level of Akt was not altered, but that of phosphorylated Akt (p-Akt, active form) was higher in hepatomas (Fig. 4B). PI3K/Akt pathway downregulates gluconeogenic enzymes by suppressing the transcription factor, FoxO1 [25]. FoxO1 in hepatomas was downregulated based on a lower protein level and a higher ratio of p-FoxO1/FoxO1 compared to the liver (Fig. 4B).

3.5. Production of serine and glycine, but not lactate, is increased in hepatomas

Pyruvate can be converted to lactate or alanine instead of entering the TCA cycle (Fig. 5A). Lactate concentration was not higher in hepatomas compared to non-malignant surrounding liver tissue, but it was slightly higher compared to the liver of healthy rats. The fraction of ^{13}C-labeled lactate was lower in hepatomas compared to the liver (Fig. 3B), and gene expression of LDHA was also reduced (Fig. 5C–D). Similarly the concentration of alanine and the fraction of ^{13}C-labeled alanine were lower in hepatomas than the liver (Table 1).

In contrast, [U-$^{13}C_3$]glycerol metabolism to serine and glycine was increased in hepatomas. Both serine and glycine concentrations were higher in hepatomas than the liver. ^{13}C-labeled serine was detected in hepatomas only, and ^{13}C-labeled glycine was much higher in hepatomas compared to the liver (Fig. 5E–F). There was exchange between

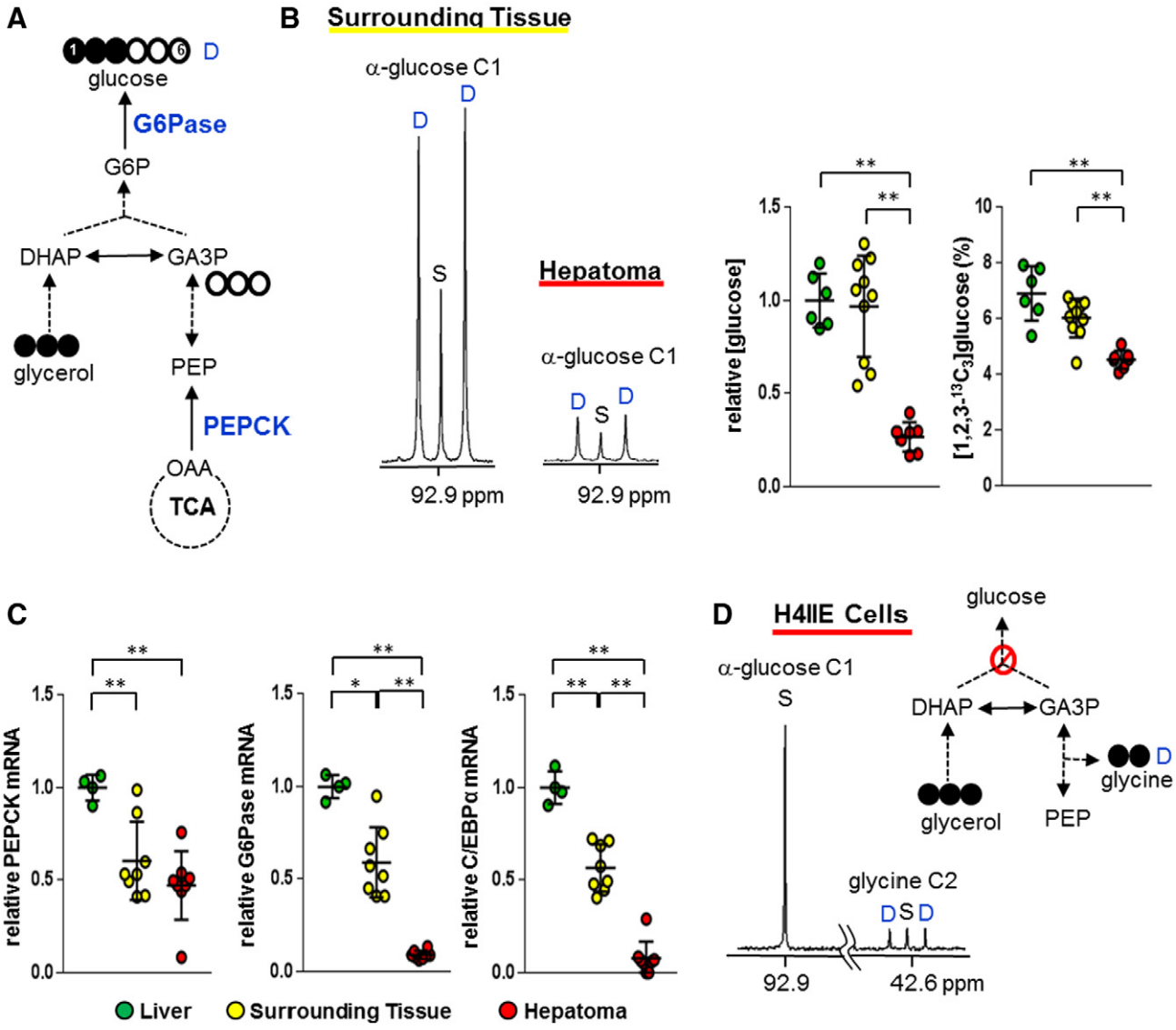

Fig. 3. Minimal gluconeogenesis in hepatomas. (A) Schematic shows gluconeogenic processes from glycerol and the TCA cycle. (B) The level of glucose and the enrichment by [1,2,3-$^{13}C_3$] glucose are lower in hepatomas compared to the liver. A singlet (S) is signal from natural ^{13}C abundance and a doublet (D) is signal from [1,2,3-$^{13}C_3$]glucose. (C) PEPCK, G6Pase and C/EBPα mRNA expressions all are reduced in hepatomas. (D) H4IIE cells were treated with [U-$^{13}C_3$]glycerol, and ^{13}C NMR of the cell extracts shows signals from glucose and glycine. A doublet is observed in glycine only, informing [U-$^{13}C_3$]glycerol metabolism to glycine, but not to glucose. Abbreviations: D, doublet from coupling of ^{13}C with adjacent ^{13}C; S, singlet; open circle = ^{12}C; black circle = ^{13}C; *, $p < 0.05$; **, $p < 0.001$; data are represented as mean ± SD.

serine and glycine in hepatomas as evidenced by ^{13}C-labeling patterns in these molecules (Fig. S2). As illustrated in Fig. 5A, enzymes involved in glycine metabolism were examined including 3-phosphoglycerate dehydrogenase (PHGDH), phosphoserine aminotransferase (PSAT), serine hydroxymethyltransferase (SHMT), and glycine decarboxylase (GLDC). Both PHGDH and PSAT1 mRNA expressions were increased by ~20 fold in hepatomas, but SHMT1/2 and GLDC were reduced (Fig. 5G).

The high level of serine in hepatomas may play a contributory role in pyruvate decarboxylation. Serine is an allosteric activator of pyruvate kinase (PK) M2 [26], and PKM2 protein was detected in hepatomas only (Fig. 5D). However, the lack of p-PKM2 in tumors (Fig. 5D) reflects the presence of active tetrameric PKM2, which was reported to drive pyruvate into the TCA cycle through PDH for oxidative phosphorylation [27–29].

4. Discussion

We studied metabolic alterations in orthotopic hepatomas of rats using multiple complementary technologies, [U-$^{13}C_3$]glycerol as a tracing molecule with ^{13}C NMR analysis of downstream metabolites, enzyme expression quantitation, and phosphorylation states of relevant enzymes. We demonstrated that pyruvate entry into the TCA cycle in hepatomas occurred exclusively through PDH followed by oxidation in the TCA cycle. In contrast, pyruvate in the liver was metabolized predominantly via pyruvate carboxylation followed by gluconeogenesis, consistent with the fasted state of these animals. Glycerol metabolism to lactate was modest, but metabolism to serine and glycine was enhanced in hepatomas. The increase in PDH activity was attributed to downregulated PDK2/4. Conversely, reduced gluconeogenesis and reduced expressions of gluconeogenic enzymes in hepatomas were consistent with an increase in phosphorylated FoxO1 linked to the Akt pathway.

Metabolic processes in orthotopic hepatomas differed not only from the liver but also from the behavior of many other tumor cells reported previously, in several important respects. *First*, earlier reports indicated that PDH activity was attenuated in cancer cells by multiple factors including a high ratio of acetyl-CoA/CoA due to persistent fatty acid β-oxidation and consequent suppression of PDH activity [30]. The suppressed PDH was associated with upregulated PDK1 [30,31]. In contrast, in the current study, PDK1 expression was unchanged and PDK2/4 was downregulated. The anticipated metabolic consequence in vivo, enhanced PDH activity, was readily confirmed by ^{13}C NMR analysis. *Second*, modest lactate production and downregulated LDH in the hepatomas were quite different from most tumors. The combination of high pyruvate level and high NADH/NAD ratio in most tumors was associated with reduced oxidation of pyruvate through the TCA cycle and diversion of pyruvate to lactate. This hallmark of cancer was confirmed by our previous studies in orthotopic hepatomas produced using N1S1 cells [32] or H4IIE cells (not published) with the use of ^{13}C-glucose. The same animal model was used in the current study, but lactate over-production was not detected in hepatomas after ^{13}C-glycerol administration. *Third*, PKM2 in hepatomas was present in the active (dephosphorylated) form. This finding is distinct from most cancers where PKM2 is largely phosphorylated. Phosphorylated PKM2 has

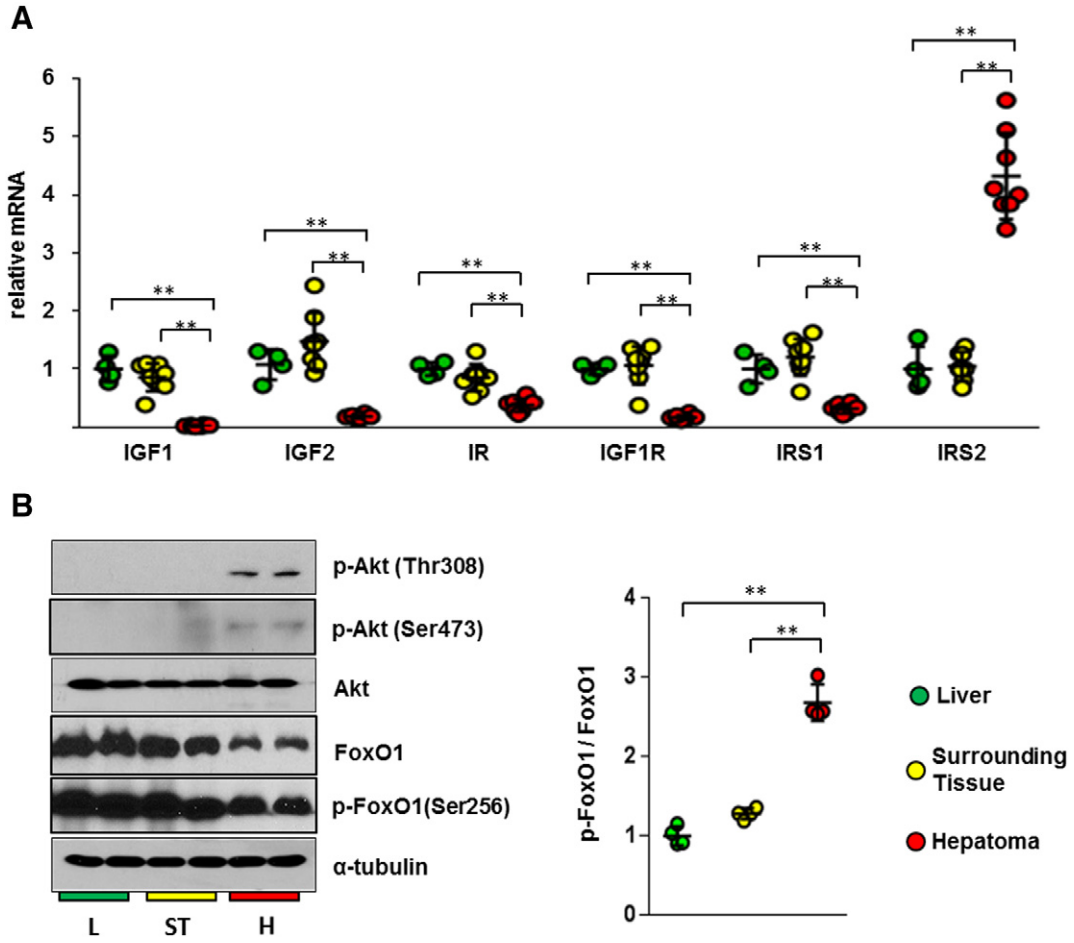

Fig. 4. Suppressed FoxO1 by Akt in hepatomas. (A) Hepatomas have higher gene expression of IRS2, but lower expressions of IGF1, IGF2, IR, IGF1R and IRS1 compared to the liver. (B) The proteins of p-Akt (Thr308) and p-Akt (Ser473) are detected in hepatomas only while the protein of Akt remains unchanged. FoxO1 protein is lower, but the ratio of p-FoxO1/FoxO1 is higher in hepatomas compared to the liver. Active Akt downregulates FoxO1 in hepatomas, which suppresses gluconeogenesis. **, $p < 0.001$; data are represented as mean ± SD.

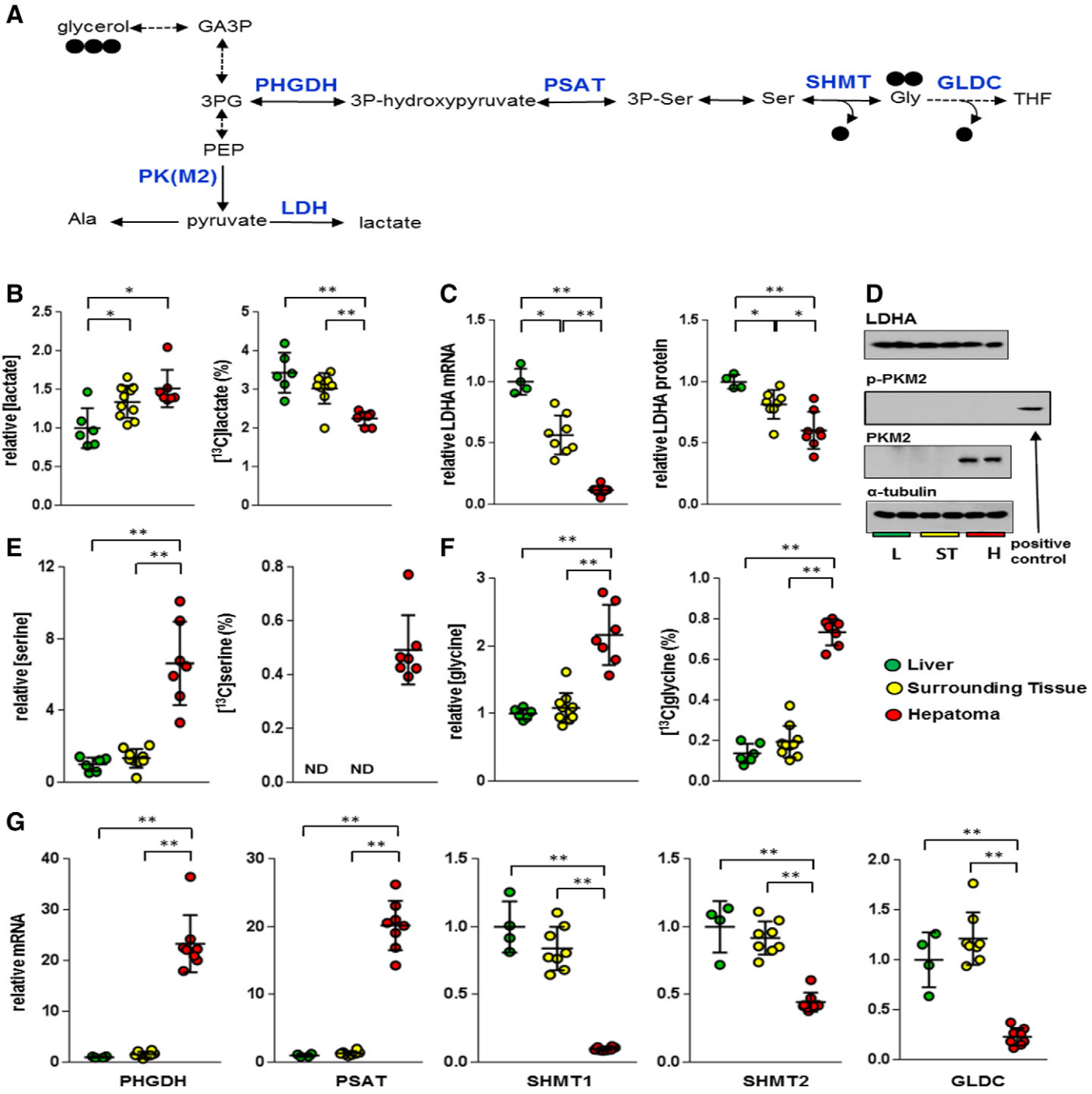

Fig. 5. Moderate lactate production, but enhanced serine and glycerol in hepatomas. (A) Schematic shows [U-$^{13}C_3$]glycerol metabolism to lactate and glycine. (B) Lactate concentration is slightly higher, but its ^{13}C enrichment is lower in hepatomas compared to the liver. (C–D) Protein and mRNA expression of LDHA are lower in hepatomas compared to the liver. PKM2 protein is detected in hepatomas only, but p-PKM2 protein is not detected in hepatomas. (E) Serine concentration is higher in hepatomas compared to the liver and ^{13}C-labeled serine is detected in hepatomas only. (F) Glycine concentration and its ^{13}C enrichment are increased in hepatomas. (G) The mRNA expressions of PHGDH and PSAT are higher while the expressions of SHMT1/2 and GLDC are lower in hepatomas than the liver. Abbreviations: black circle = ^{13}C; *, $p < 0.05$; **, $p < 0.001$; data are represented as mean ± SD.

reduced affinity for phosphoenolpyruvate, presumably contributing to accumulation of glycolytic intermediates enabling biosynthetic reactions and consequently cell proliferation [27–29]. The presence of phosphorylated PKM2 in most tumors was mediated by hypoxia-inducible factor-1α (HIF-1α) and Myc [33–36]. In the current study, however, expressions of both genes were not significantly different in hepatomas compared to the liver and were consistent with our finding that PKM2 was dephosphorylated (Fig. S3A–B). Although there are other steps regulating glycerol oxidation, this finding is consistent with the observation by ^{13}C NMR that glycerol was readily oxidized in the TCA cycle via PDH. *Finally*, the expression of GLDC in the current study was reduced in hepatomas, again differing from most tumors [37,38]. GLDC is required for the transfer of methyl group of glycine to one-carbon metabolism for nucleotide synthesis [39], but it was downregulated in hepatomas. Inhibition of glycine metabolism at this step is consistent with the increased concentration of serine and glycine in hepatomas. In this study, regulation of PKM2, PDH, LDH and glycine metabolism were examined by gene expression or measurements of phosphorylation states of the relevant enzymes. In all instances, the predicted metabolic effects in hepatomas were confirmed by isotope tracing in vivo.

The loss of gluconeogenesis in hepatomas was evidenced by multiple data. No glucose production from the TCA cycle could be detected. Somewhat surprisingly, since glucose production from glycerol is a relatively simple pathway requiring little energy, gluconeogenesis from glycerol could not be detected in hepatomas, either. This is consistent with previous reports about downregulated gluconeogenic enzymes in hepatoma cells, but not fully consistent with a study using isolated, tumor-bearing livers [18]. The latter study reported impaired gluconeogenesis from pyruvate and alanine, like the current results, but preserved gluconeogenesis from glycerol. The absence of gluconeogenesis from glycerol is a straightforward result of the current study. However, direct comparison between two studies may not be reasonable due to differences in methods including cell lines. Also, the earlier study did not distinguish hepatoma metabolism from non-malignant surrounding liver tissue metabolism. The regulation of gluconeogenesis by FoxO1 is known [25], and the minimal gluconeogenesis in hepatomas was attributed to suppressed FoxO1 by active Akt. The PDH activity in hepatomas could be also attributed to Akt because of reported Akt regulation in PDHE1 phosphorylation [40,41].

Overall the results from gene expression and phosphorylation state were consistent with results from ^{13}C isotope analysis. There were, however, a few exceptions. In principle, both PDP and PDK modulate phosphorylation of PDHE1, but downregulated PDP2 in spite of active PDH in hepatomas indicated that PDP2 was not critical in controlling the activity under these conditions. The discrepancy between downregulated SHMT1/2 and enhanced metabolism to glycine was also detected in hepatomas, and this could be explained partially by suppressed glycine cleavage by downregulated GLDC (Fig. 5G).

In summary, analysis of the products from metabolism of [U-$^{13}C_3$] glycerol provided a detailed window of multiple pathways in hepatomas as well as the liver. We demonstrated unexpected changes in orthotopic hepatomas with the use of the glycerol including upregulated PDH, downregulated LDH, downregulated GLDC and dephosphorylated PKM2. These findings need to be validated using other models or preferably with human patients because only a single cell line was used to produce rodent models in this study. The major findings in this study are directly related to recent strategies proposed for cancer treatment that target reprogrammed metabolism. Directing lactate for oxidative phosphorylation through PDH arrested many cancer cells including hepatomas and human brain tumors, and PDK inhibitors such as dichloroacetate have been developed to activate PDH [10,42,43]. Inhibiting GLDC is another strategy to arrest cell proliferation since its activity is required for de novo purine synthesis [39]. Here hepatomas after the administration of glycerol revealed multiple potential pathways that may be targets for anticancer therapies, and glycerol is acceptable for administration to human patients. Since ^{13}C is a stable isotope, extension of this exam to human patients is straightforward.

Acknowledgements

We thank Rebecca Murphy and Thomas Hever for technical support, and Dr. Jian-xiong Wang for MRI acquisition.

Authors' contributions

Conceptualization, MHL, RJD, CRM, and ESJ; Methodology, MHL, XW, and ESJ; Investigation, MHL, XW, IRC and ESJ; Writing - Original Draft, MHL and ESJ; Writing-Review & Editing, RJD, ADS, CRM, and ESJ; Funding Acquisition, CRM and ESJ.

Funding

This study was supported by the National Institutes of Health [DK099289 to ESJ, DK058398 and EB015908 to CRM].

Declaration of competing interest

The authors declare no competing interests.

Appendix A. Supplementary data

Supplementary data to this article can be found online at https://doi.org/10.1016/j.metabol.2019.153993.

References

[1] Vander Heiden MG, Cantley LC, Thompson CB. Understanding the Warburg effect: the metabolic requirements of cell proliferation. Science 2009;324:1029–33. https://doi.org/10.1126/science.1160809.
[2] López-Lázaro M. The Warburg effect: why and how do cancer cells activate glycolysis in the presence of oxygen? Anticancer Agents Med Chem 2008;8:305–12. https://doi.org/10.2174/187152008783961932.
[3] DeBerardinis RJ, Mancuso A, Daikhin E, Nissim I, Yudkoff M, Wehrli S, et al. Beyond aerobic glycolysis: transformed cells can engage in glutamine metabolism that exceeds the requirement for protein and nucleotide synthesis. Proc Natl Acad Sci U S A 2007;104:19345–50. https://doi.org/10.1073/pnas.0709747104.
[4] Beyoglu D, Imbeaud S, Maurhofer O, Bioulac-Sage P, Zucman-Rossi J, Dufour JF, et al. Tissue metabolomics of hepatocellular carcinoma: tumor energy metabolism and the role of transcriptomic classification. Hepatology 2013;58:229–38. https://doi.org/10.1002/hep.26350.
[5] Cohen SM. ^{13}C NMR study of effects of fasting and diabetes on the metabolism of pyruvate in the tricarboxylic acid cycle and the utilization of pyruvate and ethanol in lipogenesis in perfused rat liver. Biochemistry 1987;26(2):581–9. https://doi.org/10.1021/bi00376a033.
[6] Katz J. Determination of gluconeogenesis in vivo with ^{14}C-labeled substrates. Am J Physiol 1985;248:R391–9. https://doi.org/10.1152/ajpregu.1985.248.4.R391.
[7] Jin ES, Moreno KX, Wang JX, Fidelino L, Merritt ME, Sherry AD, et al. Metabolism of hyperpolarized [1-^{13}C]pyruvate through alternate pathways in rat liver. NMR Biomed 2016;29(4):466–74. https://doi.org/10.1002/nbm.3479.
[8] Fernandez CA, Des Rosiers C. Modeling of liver citric acid cycle and gluconeogenesis based on ^{13}C mass isotopomer distribution analysis of intermediates. J Biol Chem 1995;270:10037–42. https://doi.org/10.1074/jbc.270.17.10037.
[9] Byun JK, Choi YK, Kang YN, Jang BK, Kang KJ, Jeon YH, et al. Retinoic acid-related orphan receptor alpha reprograms glucose metabolism in glutamine-deficient hepatoma cells. Hepatology 2015;61:953–64. https://doi.org/10.1002/hep.27577.
[10] Shen YC, Ou DL, Hsu C, Lin KL, Chang CY, Lin CY, et al. Activating oxidative phosphorylation by a pyruvate dehydrogenase kinase inhibitor overcomes sorafenib resistance of hepatocellular carcinoma. Br J Cancer 2013;108:72–81. https://doi.org/10.1038/bjc.2012.559.
[11] Ma R, Zhang W, Tang K, Zhang H, Zhang Y, Li D, et al. Switch of glycolysis to gluconeogenesis by dexamethasone for treatment of hepatocarcinoma. Nat Commun 2013;4:2508. https://doi.org/10.1038/ncomms3508.
[12] Levine AJ, Puzio-Kuter AM. The control of the metabolic switch in cancers by oncogenes and tumor suppressor genes. Science 2010;330(6009):1340–4. https://doi.org/10.1126/science.1193494.
[13] Kumashiro N, Beddow SA, Vatner DF, Majumdar SK, Cantley JL, Guebre-Egziabher F, et al. Targeting pyruvate carboxylase reduces gluconeogenesis and adiposity and improves insulin resistance. Diabetes 2013;62:2183–94. https://doi.org/10.2337/db12-1311.
[14] Hammond KD, Balinsky D. Activities of key gluconeogenic enzymes and glycogen synthase in rat and human livers, hepatomas, and hepatoma cell cultures. Cancer Res 1978;38:1317–22.
[15] Iansante V, Choy PM, Fung SW, Liu Y, Chai JG, Dyson J, et al. PARP14 promotes the Warburg effect in hepatocellular carcinoma by inhibiting JNK1-dependent PKM2 phosphorylation and activation. Nat Commun 2015;6:7882. https://doi.org/10.1038/ncomms8882.
[16] Kitamura K, Hatano E, Higashi T, Narita M, Seo S, Nakamoto Y, et al. Proliferative activity in hepatocellular carcinoma is closely correlated with glucose metabolism but not angiogenesis. J Hepatol 2011;55:846–57. https://doi.org/10.1016/j.jhep.2011.01.038.
[17] Chang LO, Morris HP. Enzymatic and immunological studies on pyruvate carboxylase in livers and liver tumors. Cancer Res 1973;33:2034–41.
[18] Moreira CC, Cassolla P, Dornellas AP, de Morais H, de Souza CO, Borba-Murad GR, et al. Changes in liver gluconeogenesis during the development of Walker-256 tumour in rats. Int J Exp Pathol 2013;94:47–55. https://doi.org/10.1111/iep.12002.
[19] Lin ECC. Glycerol utilization and its regulation in mammals. Annu Rev Biochem 1977;46:765–95. https://doi.org/10.1146/annurev.bi.46.070177.004001.
[20] Jones JG, Sherry AD, Jeffrey FM, Storey CJ, Malloy CR. Sources of acetyl-CoA entering the tricarboxylic acid cycle as determined by analysis of succinate ^{13}C isotopomers. Biochemistry 1993;32:12240–4. https://doi.org/10.1021/bi00096a037.
[21] Holness MJ, Sugden MC. Regulation of pyruvate dehydrogenase complex activity by reversible phosphorylation. Biochem Soc Trans 2003;31:1143–51. https://doi.org/10.1042/bst0311143.
[22] Kolobova E, Tuganova A, Boulatnikov I, Popov KM. Regulation of pyruvate dehydrogenase activity through phosphorylation at multiple sites. Biochem J 2001;358:69–77. https://doi.org/10.1042/0264-6021:3580069.

[23] T.E. Roche , J.C. Baker, X. Yan, Y. Hiromasa , X. Gong, T. Png, et al. Distinct regulatory properties of pyruvate dehydrogenase kinase and phosphatase isoforms. Prog. Nucleic Acid Res Mol Biol. 2001;70:33–75.
[24] Pedersen TA, Bereshchenko O, Garcia-Silva S, Ermakova O, Kurz E, Mandrup S, et al. Distinct C/EBPalpha motifs regulate lipogenic and gluconeogenic gene expression in vivo. EMBO J 2007;26:1081–93. https://doi.org/10.1038/sj.emboj.7601563.
[25] Nakae J, Kitamura T, Silver DL, Accili D. The forkhead transcription factor Foxo1 (Fkhr) confers insulin sensitivity onto glucose-6-phosphatase expression. J Clin Invest 2001;108(9):1359–67. https://doi.org/10.1172/JCI12876.
[26] Chaneton B, Hillmann P, Zheng L, Martin AC, Maddocks OD, Chokkathukalam A, et al. Serine is a natural ligand and allosteric activator of pyruvate kinase M2. Nature 2012;491:458–62. https://doi.org/10.1038/nature11540.
[27] N. Wong, J. De Melo , D. Tang. PKM2, a central point of regulation in cancer metabolism. Int J Cell Biol 2013;2013: 242513. https://doi.org/10.1155/2013/242513.
[28] Christofk HR, Vander Heiden MG, Wu N, Asara JM, Cantley LC. Pyruvate kinase M2 is a phosphotyrosine-binding protein. Nature 2008;452:181–6. https://doi.org/10.1038/nature06667.
[29] T. Hitosugi, S. Kang, M.G. Vander Heiden, T.W. Chung, S. Elf, K. Lythgoe, et al. Tyrosine phosphorylation inhibits PKM2 to promote the warburg effect and tumor growth. Sci Signal. 2009;2:ra73. https://doi.org/10.1126/scisignal.2000431
[30] Biswas S, Lunec J, Bartlett K. Non-glucose metabolism in cancer cells–is it all in the fat? Cancer Metastasis Rev 2012;31:689–98. https://doi.org/10.1007/s10555-012-9384-6.
[31] J.W. Kim, P. Gao, Y.C. Liu, G.L. Semenza, C.V. Dang. Hypoxia-inducible factor 1 and dysregulated c-Myc cooperatively induce vascular endothelial growth factor and metabolic switches hexokinase 2 and pyruvate dehydrogenase kinase 1. Mol Cell Biol. 2007;27(21):7381–93. https://doi.org/10.1128/MCB.00440-07
[32] Lee MH, Malloy CR, Corbin IR, Li J, Jin ES. Assessing the pentose phosphate pathway using [2, 3-$^{13}C_2$]glucose. NMR Biomed 2019;32(6):e4096. https://doi.org/10.1002/nbm.4096.
[33] Kim JW, Tchernyshyov I, Semenza GL, Dang CV. HIF-1-mediated expression of pyruvate dehydrogenase kinase: a metabolic switch required for cellular adaptation to hypoxia. Cell Metab 2006;3:177–85. https://doi.org/10.1016/j.cmet.2006.02.002.
[34] Papandreou I, Cairns RA, Fontana L, Lim AL, Denko NC. HIF-1 mediates adaptation to hypoxia by actively downregulating mitochondrial oxygen consumption. Cell Metab 2006;3:187–97. https://doi.org/10.1016/j.cmet.2006.01.012.
[35] Ma X, Li C, Sun L, Huang D, Li T, He X, et al. Lin28/let-7 axis regulates aerobic glycolysis and cancer progression via PDK1. Nat Commun 2014;5:5212. https://doi.org/10.1038/ncomms6212.
[36] Le A, Cooper CR, Gouw AM, Dinavahi R, Maitra A, Deck LM, et al. Inhibition of lactate dehydrogenase A induces oxidative stress and inhibits tumor progression. Proc Natl Acad Sci USA 2010;107:2037–42. https://doi.org/10.1073/pnas.0914433107.
[37] Zhang WC, Shyh-Chang N, Yang H, Rai A, Umashankar S, Ma S, et al. Glycine decarboxylase activity drives non-small cell lung cancer tumor-initiating cells and tumorigenesis. Cell 2012;148:259–72. https://doi.org/10.1016/j.cell.2011.11.050.
[38] Locasale JW. Serine, glycine and one-carbon units: cancer metabolism in full circle. Nat Rev Cancer 2013;13:572–83. https://doi.org/10.1038/nrc3557.
[39] Jain M, Nilsson R, Sharma S, Madhusudhan N, Kitami T, Souza AL, et al. Metabolite profiling identifies a key role for glycine in rapid cancer cell proliferation. Science 2012;336:1040–4. https://doi.org/10.1126/science.1218595.
[40] Kim B, Feldman EL. Insulin receptor substrate (IRS)-2, not IRS-1, protects human neuroblastoma cells against apoptosis. Apoptosis 2009;14:665–73. https://doi.org/10.1007/s10495-009-0331-0.
[41] Cerniglia GJ, Dey S, Gallagher-Colombo SM, Daurio NA, Tuttle S, Busch TM, et al. The PI3K/Akt pathway regulates oxygen metabolism via pyruvate dehydrogenase (PDH)-E1α phosphorylation. Mol Cancer Ther 2015;14:1928–38. https://doi.org/10.1158/1535-7163.MCT-14-0888.
[42] Zhang W, Zhang SL, Hu X, Tam KY. Targeting tumor metabolism for cancer treatment: is pyruvate dehydrogenase kinases (PDKs) a viable anticancer target? Int J Biol Sci 2015;11(12):1390–400. https://doi.org/10.7150/ijbs.13325.
[43] Dunbar EM, Coats BS, Shroads AL, Langaee T, Lew A, Forder JR, et al. Phase 1 trial of dichloroacetate (DCA) in adults with recurrent malignant brain tumors. Invest New Drugs 2014;32:452–64. https://doi.org/10.1007/s10637-013-0047-4.